ACS APPLIED MATERIALS & INTERFACES

Research Article

Cite This: ACS Appl. Mater. Interfaces 2020, 12, 818−825

www.acsami.org

Cost-Effective and Semi-Transparent PbS Quantum Dot Solar Cells Using Copper Electrodes

Hadi Tavakoli Dastjerdi,[*,†] Pengfei Qi,[‡] Zhiyong Fan,[§,∥] and Mohammad Mahdi Tavakoli[*,⊥]

[†]Department of Materials Science and Engineering and [⊥]Department of Electrical Engineering and Computer Science, Massachusetts Institute of Technology, Cambridge, Massachusetts 02139, United States

[‡]Zhong Shan Rui Ke New Energy Company, Limited, 13th Torch Road, Torch Development Zone, Zhongshan City, Guangdong Province 528437, China

[§]Department of Electronic and Computer Engineering, The Hong Kong University of Science and Technology, Clear Water Bay, Kowloon, Hong Kong SAR, China

[∥]HKUST-Shenzhen Research Institute, No. 9 Yuexing First RD, South Area, Hi-tech Park, Nanshan, Shenzhen 518057, China

Supporting Information

ABSTRACT: PbS quantum dots (QDs) have gained significant attention as promising solution-based materials for third generation of photovoltaic (PV) devices, thanks to their size-tunable band gap, air stability, and low-cost solution processing. Gold (Au), despite its high cost, is the standard electrode in the conventional PbS QD PV architecture because of its perfect alignment with valence levels of PbS QDs. However, to comply with manufacturing requirements for scalable device processing, alternative cost-effective electrodes are urgently required. Here, we employed an interface engineering approach and deposited poly(3-hexylthiophene-2,5-diyl) as a hole transport layer on 1,2-ethanedithiol-capped PbS QDs in order to adjust the valence band of QDs with the work function of inexpensive copper (Cu) electrodes. In fact, this is the first report of a Au-free PbS QD PV system employing the conventional device structure. Our Cu-based device shows a maximum power conversion efficiency (PCE) of 8.7% which is comparable with that of the Au-based device (10.2%). Interestingly, the P3HT-based device shows improved stability with relatively 10% PCE loss after 230 h under continuous illumination. Moreover, using an ultrathin Cu electrode, a semitransparent PbS QD PV is fabricated with a remarkably high average visible transparency of 26% and a PCE of 7.4%.

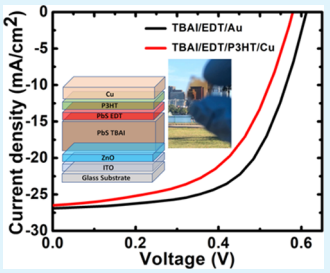

KEYWORDS: *PbS QDs, solar cell, P3HT, cost-effective, semitransparent, copper*

INTRODUCTION

Among different types of solution-processed photovoltaic (PV) systems, PbS colloidal quantum dot (QD) PVs[1−11] have attracted increasing attention because of their promising characteristics such as size-dependent band gap, impressive air-stability, and adaptability to industry-level and large-scale applications.[12−15] Most of the research studies on the PbS QD PV have focused on QDs surface passivation and enhancement of device performance through band alignment engineering to facilitate carrier extraction from the QD active layer.[1,3,6,16−18] However, in order to fulfill the industry-level production, the overall device development costs should be significantly reduced. Currently, Au is the most dominant anode material in PbS QD PVs including the best performing PbS QD PVs with a power conversion efficiency (PCE) of 12%[19] because of the compatibility of its work function level to the underlying QDs absorber layer. However, the presence of Au as the electrode in PbS QD PVs considerably increases the overall device fabrication cost, especially for large-scale production. On the other hand, employment of alternative electrode materials requires band alignment engineering to assure unimpeded hole transport to the electrode. Herein, we fabricate efficient PbS QD PV devices with copper (Cu) electrodes through introduction of a hole transporting layer (HTL) on the top of 1,2-ethanedithiol (EDT)-capped PbS QDs. EDT-capped PbS QDs act as the HTL in the currently dominant PbS QD PV architectures.[1,7,8,19] We employ a stable polymer poly(3-hexylthiophene-2,5-diyl) (P3HT) to adjust the band energy level of the QD layer with respect to the Cu electrode. P3HT is a commonly used HTL in solution-based PVs[20−22] with good stability compared to other small molecules because of its hydrophobicity and oxygen impermeability.[23] It is commonly doped with Li or Co salts to increase its hole mobility.[24,25] Because the highest occupied molecular orbital level (−4.8 to −5.1 eV) of P3HT is well-aligned with the valence band of EDT-capped PbS QDs, it can be used as an interfacial layer between the QD absorber layer and the low-cost Cu electrode, which has a lower work function compared to Au. Moreover, it has been shown before that a higher molecular weight of P3HT is advantageous[26] because by increasing the molecular weight, domain boundaries and inherent improvement of the chain length

Received: October 11, 2019
Accepted: December 10, 2019
Published: December 10, 2019

DOI: 10.1021/acsami.9b18487
ACS Appl. Mater. Interfaces 2020, 12, 818−825

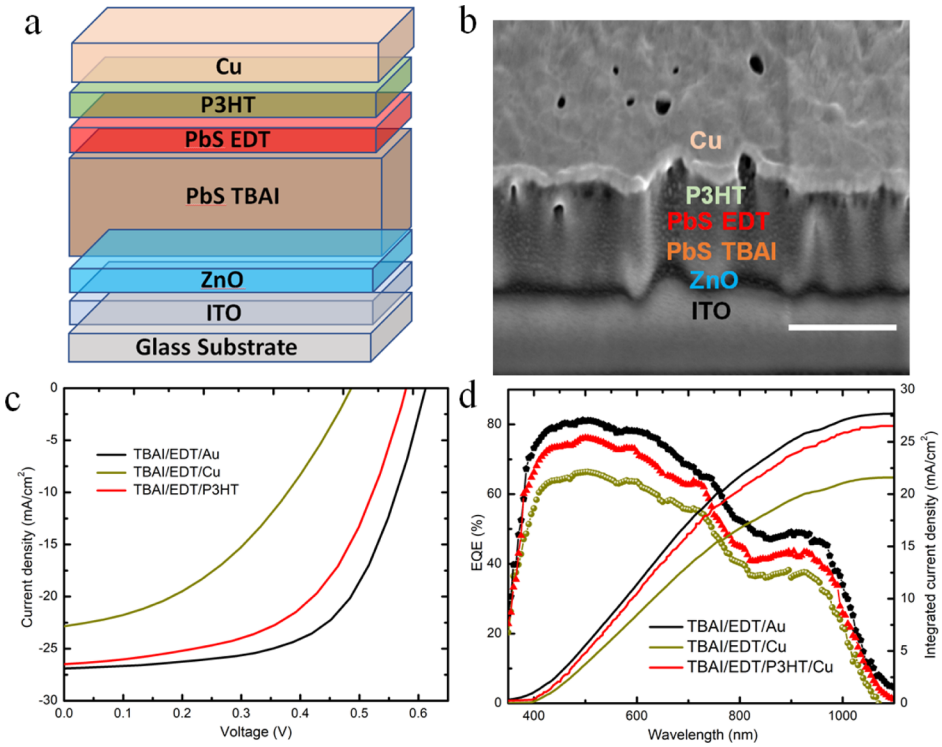

Figure 1. (a) Schematic of the PbS QDs PV device architecture. (b) FIB-milled cross-sectional SEM image of the QDs PV with P3HT and Cu electrodes (scale bar is 200 nm). (c) $J-V$ characteristics of representative devices with different electrodes with and without a P3HT interfacial layer measured under 100 mW/cm^2 illumination and AM 1.5G condition. The statistics of PV parameters for six devices are shown in Table 1. (d) EQE spectra of the devices with different electrodes with and without a P3HT interfacial layer.

Table 1. PV Characteristics of PbS QDs Devices with Au and Cu Electrodes with and without P3HT Interlayer Measured under 100 mW/cm^2 AM1.5G Illumination[a]

device	V_{OC} (mV)	J_{SC} (mA/cm^2)	FF	PCE (%)
TBAI/EDT/Au	611 ± 3	26.9 ± 0.3	0.62 ± 0.01	10.2 ± 0.2
TBAI/EDT/Cu	482 ± 6	22.7 ± 0.1	0.42 ± 0.02	4.6 ± 0.3
TBAI/EDT/P3HT/Cu	578 ± 6	26.4 ± 0.6	0.55 ± 0.02	8.4 ± 0.3

[a]Mean and standard deviations are calculated for six devices in each sample.

result in enhanced carrier transport.[27] Our Au-free PbS QD PV with Cu electrodes shows a PCE of 8.7% (vs control Au device with 10.2%). Developing semitransparent solar cells from solution-based active materials, including PbS QDs,[28,29] has also been an interesting area of research for applications in building-integrated PV.[30,31] The generally accepted requirement of average visible transparencies (AVTs)—defined as the mean optical transmittance of a device between 380 and 780 nm—for window applications is at least 25%.[32] To demonstrate the possibility of developing a semitransparent PbS QD PV out of this novel device architecture, we employed sufficiently thin QD absorber layers and an ultrathin Cu electrode. The semitransparent PbS QD PV with ultrathin Cu electrodes are presented with a remarkably high AVT of 26% and PCE of 7.4%.

RESULTS AND DISCUSSION

The schematic illustration and cross-sectional scanning electron microscopy (SEM) image of the optimum PbS QD PV with Cu electrodes and EDT-capped PbS/P3HT double HTL are shown in Figure 1a,b. The PbS QDs used in this study show an absorption peak at ∼ 950 nm as seen in Figure S1. This structure consists of indium-doped tin oxide (ITO), ZnO electron transporting layer, tetrabutylammonium iodide (TBAI)-capped PbS QDs, EDT-capped PbS QDs, P3HT HTLs, and Cu electrodes. A 40 nm-thick polycrystalline ZnO layer was deposited on the ITO-coated glass substrates using the sol–gel method (see Experimental Section). PbS QDs were then deposited via a layer-by-layer deposition technique. The ligand exchange for the first 10 QDs layers was performed using a solution of TBAI in methanol. To form the device with double HTLs, a solution of EDT in acetonitrile was used during ligand exchange for the last two PbS QD layers, followed by deposition of a 10 nm-thick Li-doped P3HT layer (See the Experimental Section for details). The Cu electrodes were then thermally evaporated through a shadow mask to complete the device structure. To study the impact of the Cu electrode and the additional P3HT HTL, we first compared the performance of the PbS-TBAI/PbS-EDT/Cu device with that of the PbS-TBAI/PbS-EDT/Au one. The PbS-TBAI/PbS-EDT/Au device shows an open circuit voltage (V_{OC}) of 611 mV, a short circuit current density (J_{SC}) of 26.9 mA/cm^2, and a fill factor (FF) of 0.62, resulting in a PCE of 10.2%. In contrast, the PbS-TBAI/PbS-EDT/Cu device shows significantly lower PV parameters, a V_{OC} of 482 mV, a J_{SC} of 22.7 mA/cm^2, a FF of 0.42, and a PCE of 4.6%. We attribute

DOI: 10.1021/acsami.9b18487
ACS Appl. Mater. Interfaces 2020, 12, 818–825

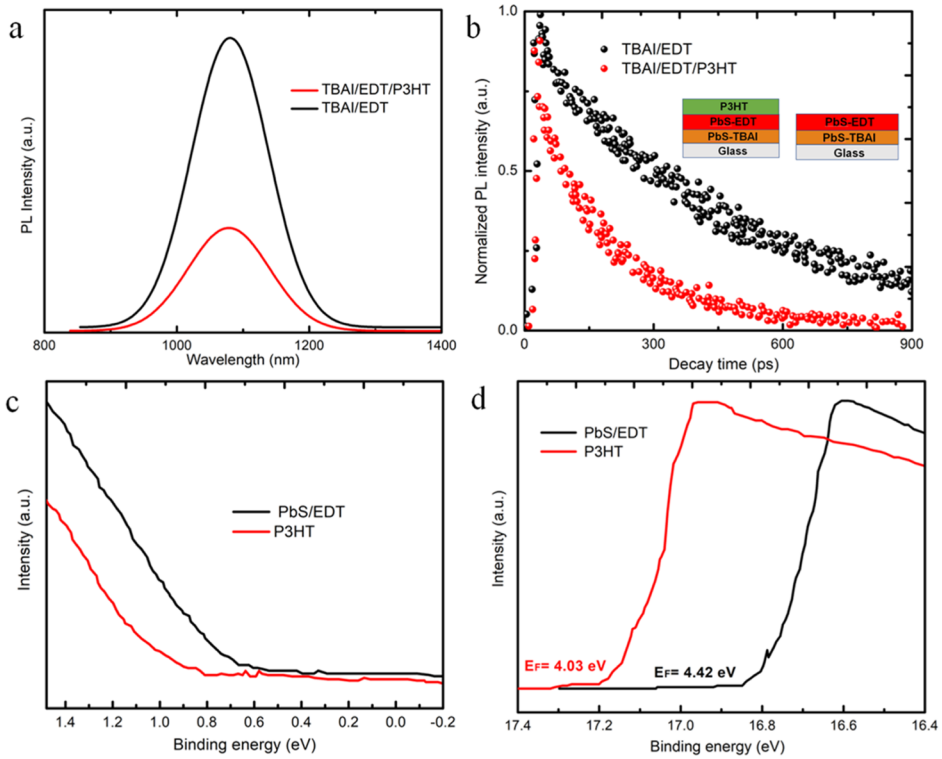

Figure 2. PL spectra of PbS QDs with and without P3HT HTL showing noticeable PL quenching for QDs with P3HT layers. (b) TRPL decay of PbS-TBAI QDs films with the PbS-EDT and PbS-EDT/P3HT HTLs. (c) Magnified UPS spectra of EDT-capped PbS QDs and P3HT layers near the Fermi edge. (d) UPS secondary electron cut-offs of the EDT-capped PbS QDs and P3HT layers. The measured Fermi levels with respect to the vacuum level are indicated on corresponding films.

this low PCE to the significantly lower work function of Cu compared to Au, which impedes hole transfer to the anode electrode. To improve the hole extraction of the PbS-TBAI/PbS-EDT/Cu structure, we inserted a P3HT HTL between the PbS QDs-EDT and the Cu electrode to adjust the band alignment between the HTL and the Cu electrode properly. Figure 1c shows the current density−voltage (J−V) characteristics of the representative PVs, measured under a simulated sun with 100 mW/cm^2 and AM1.5MG conditions. Compared to the PbS-TBAI/PbS-EDT/Cu structure, the PbS-TBAI/PbS-EDT/P3HT/Cu structure shows noticeably improved PV parameters, as shown in Figure 1c. Further optimization of P3HT concentration results in an optimized device with a V_{OC} of 578 mV, a J_{SC} of 26.4 mA/cm^2, and a FF of 0.55, resulting in a PCE of 8.4%, which is significantly better than the PbS-TBAI/PbS-EDT/Cu device with only 4.6% PCE (see Table 1 for more details). Figure 1d shows the external quantum efficiency (EQE) spectra of the representative devices and their corresponding integrated short-circuit current densities (J_{SC}). The integrated J_{SC} calculated from the EQE results (Figure 1d) are in good agreement with the J−V measurements.

Figure 2a,b shows static photoluminescence (PL) and time-resolved photoluminescence (TRPL) spectra of PbS-TBAI/PbS-EDT (control) and the optimized PbS-TBAI/PbS-EDT/P3HT films spin-coated on a glass substrate. PL and TRPL spectra of the PbS/TBAI were taken by shining the laser from the glass side in both samples to monitor the impact of having the P3HT layer. Significant PL quenching is observed for the PbS-TBAI/PbS-EDT/P3HT film as shown in Figure 2a, indicating an improved charge transfer from the QD layer to the HTL because of reduced radiative recombination between the electron and the holes in the absorber layer. This effect has been widely reported for HTLs used in various types of absorber materials.[33−35] Decreased carrier lifetime (see Table S1, Supporting Information) and significant PL quenching of the PbS-TBAI/PbS-EDT/P3HT as compared to the control film suggest improved charge separation at the interface.

Improved PV performance of the device with the P3HT HTL compared to that of the control device suggests improved band alignment between the QD layer and the Cu electrode. To assess the energy band levels of the PbS-TBAI, PbS-EDT, and P3HT, ultraviolet photoelectron spectroscopy (UPS) was performed on each layer (see Figure 2c,d). The energy band diagrams of both structures, upon extraction of valence band maxima and Fermi energy levels of the corresponding films, are calculated and plotted as shown in Figure 3a. The impeded hole transport from the PbS-EDT HTL to Cu is due to a relatively large energy barrier between the valence band of the PbS-EDT and the work function of Cu, which can be inferred from Figure 3a. This condition is relaxed for the structure with the inserted second HTL (P3HT), which facilitates hole transfer to the relatively low work function of Cu electrodes and leads to improved diode characteristics and overall PV performance.

The representative semilog dark J−V characteristics shown in Supporting Information Figure S2 confirm the improvement of the diode characteristics upon inserting the P3HT HTL into the structure. Significant reduction of leakage current for the double HTL PV indicates enhanced hole selectivity of the Cu electrode upon adding the P3HT HTL. We attribute the lower series resistance (see Table S2, Supporting Information) of the double HTL PV to the lower energy barrier between the double HTL and work function of

DOI: 10.1021/acsami.9b18487
ACS Appl. Mater. Interfaces 2020, 12, 818−825

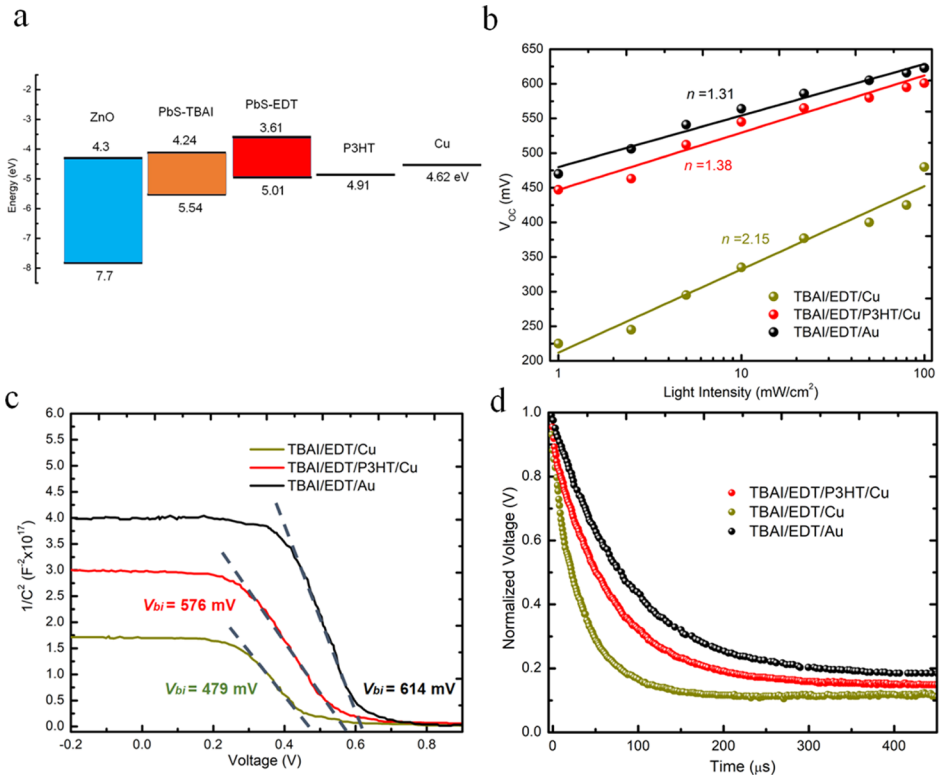

Figure 3. (a) Energy-level diagram of the PbS QD solar cells with P3HT with respect to the vacuum level, plotted from the UPS results shown in Figure 2c,d. (b) V_{OC} as a function of light intensity for reference devices as well as devices with a Cu electrode with and without a P3HT interlayer. (c) Capacitance–voltage measurements for the built-in potential of PbS QD devices with and without a P3HT interlayer and for the reference device. (d) TPV decay measurements of the PbS QDs devices with and without the P3HT interlayer and the reference device at open-circuit conditions under 1 sun light bias.

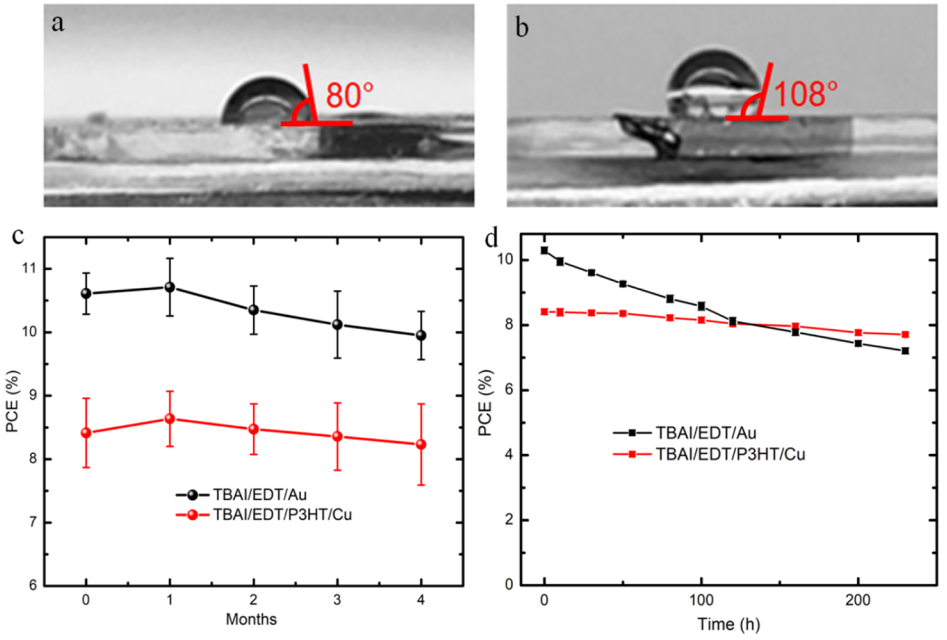

Figure 4. CA measurements of (a) PbS-EDT film and (b) P3HT film. Evolution of PCE in (c) long-term stability measurement of PbS QDs solar cells in ambient conditions with 40% relative humidity and (d) photostability measurement of PbS QD solar cells with Au and Cu electrodes under continuous illumination.

Cu. Regular structures of PbS QD PVs usually have a noticeable density of pinholes inside the structure,[36] which are potential pathways for parasitic current passage after electrode deposition due to the diffusion of electrode metal inside the absorber layer, leading to lower shunt resistance. Therefore, the relatively higher shunt resistance of the double HTL PV is likely due to improved coating of the QD surface with P3HT resulting in less metal diffusion inside the QDs.

DOI: 10.1021/acsami.9b18487
ACS Appl. Mater. Interfaces 2020, 12, 818–825

To further validate the reduced carrier recombination as a result of facilitated hole transfer using the double HTL, the variations of V_{OC} versus illuminated light density were studied following the relation: $V_{OC} \propto nkT/q$, where n is the diode ideality factor, q is elementary charge, T is the temperature, and k is the Boltzmann constant.[5] The n values of the control and optimized double-layer HTL PVs were calculated by fitting the V_{OC}-light intensity curves as shown in Figure 3b. The extracted n value for the double HTL device is 1.38, which is noticeably lower than that of the control device (2.15). We attribute this to reduced carrier recombination in the absorber layer as a result of promoted hole transfer via using the PbS-EDT/P3HT double-layer HTL. The increase in the built-in potential of the double-layer HTL PV is also confirmed by capacitance−voltage measurements as shown in Figure 3c.

Transient photovoltage (TPV) characterization data of the control and double-layer HTL PVs are shown in Figure 3d. The device with P3HT shows rapid voltage decay (t = 38.9 μs) compared to the control device (t = 83.6 μs). This further proves the stronger career quenching effect as a result of P3HT addition, which facilitated the hole transfer.

Figure 4a and b shows the contact angles (CAs) of water droplets on the surface of PbS-EDT and P3HT films, respectively. As seen, the CAs of 80 and 108° were estimated for the EDT-capped PbS QDs and the P3HT film, respectively. The higher CA in the P3HT film demonstrates its higher hydrophobicity, which leads to increased moisture resistance and overall extended device stability in a humid environment. To validate this point, we studied the long-term stability of the devices as it is a critical step for the scope of commercialization. The long-term stability of double HTL PVs with Cu anodes is found to be superior to that of the device with Au electrode over 4 months, as shown in Figure 4c. Notably, the devices were kept in a dry box with a relative humidity of 40% for this measurement. The superior stability of the devices with P3HT under relatively humid storage conditions can be attributed to the higher hydrophobicity of P3HT as compared to that of PbS QDs without P3HT. These stability results are compared with those reported by Kirmani et al.,[14] in which they studied the role of air humidity on the performance and stability of the PbS QD PVs. They stored the devices in a dry-air box following fabrication and showed that their performance and stability improved because of oxygen doping of the PbS/EDT layer. Our P3HT devices show remarkable device stability after 4 month storage under ambient conditions with only about 10% reduction in the PCE, which is comparable to the results reported in the mentioned study. Moreover, we studied the device stability under continuous illumination for standard PbS-TBAI/PbS-EDT/Au and PbS-TBAI/PbS-EDT/P3HT/Cu PVs as shown in Figures 4d and S3. The rate of PCE reduction is lower for the devices with Cu electrodes compared to the reference cells. We attribute this to gradual diffusion of Au into PbS QDs through existing pinholes in the structure leading to reduced shunt resistance which adversely impacts the FF and V_{OC} as shown in Figure S3. This condition is relaxed for PVs with Cu electrodes because P3HT covers the surface of the QDs and blocks pathways for Au diffusion. Moreover, we believe that it should be possible to apply this method to device structures with other active materials, including PbSe QDs, such as PVs reported by Hu et al.[37] Despite the use of PbSe QDs in their device structure, they utilized a PbS/EDT HTL. Therefore P3HT/Cu should, in principle, be matched with the PbS/EDT layer used in PbSe QD PVs to replace Au electrode.

To demonstrate the possibility of developing a semitransparent PbS QD PV with the cost-effective Cu anode electrode, we fabricated the PbS QD PV with a 10 nm-thick Cu electrode. To obtain decent optical transmittance and device performance, the thickness of the QD absorber layer should be thin enough for high optical transmittance and thick enough for sufficient light absorption. Therefore, we fabricated PbS QD PVs (using P3HT and a 10 nm-thick Cu electrode) with different thicknesses of the QD layer, varying from 120 to 200 nm as shown in Table S3. The transmittance spectra of PbS QD PV devices with different thicknesses of the QD layer are shown in Figure 5a. As expected, by reducing the QD thickness from 200 to 120 nm, the PV performance drops from 8.4 to 6%, whereas the AVT increases from 24.09 to 28.33%. The semitransparent solar cell—shown in Figure 5b—was measured with illumination from both ITO and Cu sides, and the corresponding PV metrics are shown in Table S4. For the PbS QD PV with QD thickness of 150 nm, when illuminated from the ITO side, a PCE of 7.4% together with an AVT of 26% was achieved with a V_{OC} of 579 mV, a J_{SC} of 23.7 mA/cm^2, and a FF of 0.54. These values are among the best values reported in the literature, as shown in Figure S4. However, upon illumination from the Cu side, a PCE of 5.9% with a V_{OC} of 574 mV, a J_{SC} of 21.3 mA/cm^2, and a FF of 0.48 was obtained. We attribute the reduced PV performance of the device upon illumination from Cu side to optical absorption of the P3HT layer and also the lower transmittance of 10 nm thick Cu as compared to the ITO electrode, possibly because of higher optical reflection at the Cu−air interface and increased optical absorption of Cu in the infrared range.

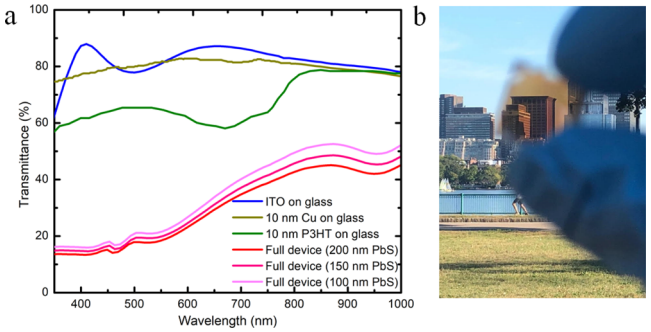

Figure 5. (a) Transmittance spectra of ITO glass, 10 nm Cu on glass, 10 nm-thick P3HT on glass and fully fabricated semitransparent devices with 10 nm thick Cu and different PbS QD thicknesses. (b) Photograph taken through the full PbS QD PV device with ultrathin Cu anode electrodes.

CONCLUSIONS

In summary, we demonstrate a low-cost and efficient PbS QDs solar cell with conventional architecture employing a Cu electrode using band alignment engineering with a stable HTL, that is, P3HT. Using this approach, we replace the expensive Au electrode in the PbS QD device with Cu and also optimize the thickness of P3HT in order to achieve the highest efficiency. Using 10 nm thick P3HT, we obtain a device with a PCE of 8.7% which is comparable with the Au-

DOI: 10.1021/acsami.9b18487
ACS Appl. Mater. Interfaces 2020, 12, 818−825

based device. Additionally, using a thin layer of Cu, semitransparent PbS QD PVs with AVT of 26% and PCE of 7.4% was developed. Interestingly, our Cu-based device shows improved stability under illumination as compared to the device with the Au electrode.

EXPERIMENTAL SECTION

PbS QD Device Fabrication. A layer of ZnO (30 nm) is deposited on pre-patterned ITO/glass substrates of a solution of ethanolamine (0.3 M) and zinc acetate dehydrate (0.3 M) in 2-methoxyethanol by spin-coating inside a nitrogen-filled glovebox. The samples were subsequently annealed at 230 °C for 15 min under ambient conditions. Synthesis of PbS QDs (capped with oleic acid) with the first absorption peak at ∼950 nm was performed according to literature.[38−42] PbS QDs with a concentration of 50 mg/mL in octane were deposited on the samples via a layer-by-layer method at 1500 rpm for 25 s leading to ∼20 nm for each QD layer. Ligand exchange was performed via a solution of TBAI (Sigma-Aldrich, 10 mg/mL in methanol) and 1,2-EDT (Sigma-Aldrich) in acetonitrile. For the device with 200 nm thickness of the PbS QD layer, 8 layers of TBAI-exchanged and 2 layers of EDT-exchanged were deposited. For thinner devices, the two layers of PbS-EDT were kept and the overall QD thickness was controlled by adjusting the thickness of PbS-TBAI layers. Ligand exchange was done by dispensing the ligand solution on the QD layer, waiting for 30 s, followed by rinsing three times with corresponding solvents and a final dry-spin. QDs deposition and ligand exchange was done under ambient conditions. P3HT was purchased from Ossila Ltd. and its molecular weight is 60.15 kDa. For the device with P3HT, a solution of P3HT dissolved in chlorobenzene (8 mg/mL) was prepared and mixed with 2.78 μL of 4-*tert*-butyl pyridine and 1.6 μL of lithium bis-(trifluoromethanesulfonyl)imide solution (520 mg/mL in acetonitrile). The P3HT solution was spin-coated at 4000 rpm for 20 s. The current price of Cu and Au are about 0.37$/g and 74$/g, respectively. Although the cost of P3HT is relatively high at about $400/g, but because we use a very small amount (8 mg/mL) for a single layer of P3HT in our device structure, the overall cost is still lower than Au. Metallic electrodes (Cu and Au from Kurt J. Lesker, 99.999%) were evaporated on the sample through a shadow mask (at 1 Å/s rate and base pressure of 10^{-6} Torr). The device area for individual solar cells was 0.054 cm^2.

Film Characterization. The optical transmittance and absorbance spectra were recorded using a UV/vis/NIR spectrometer (Lambda 1050). PL spectra were measured using a SpectraPro 300i spectrometer equipped with a liquid nitrogen-cooled indium gallium arsenide (InGaAs) detector. TRPL measurements were done by using a picosecond pulsed diode laser (EPL-405) with an excitation at λ = 405 nm and a pulse width of 49 ps. The measurements were fitted using the exponential relation: $I(t) = a_i \exp(-t/\tau_i)$, where a_i and τ_i are the amplitude and the lifetime values of each term, respectively. An FEI Helios NanoLab 600 SEM system was used (5 kV) for SEM imaging. Cross-section images were acquired via Ga-focused ion beam (FIB) milling at 30 kV using the same tool. UPS data were recorded using an Omicron ultrahigh vacuum system using the He I line (21.2 eV) of a helium discharge lamp to study the valence bands and Fermi levels of the different thin films.

Device Characterization. A semiconductor device analyzer (Agilent Technologies, B1500A) was used to record current−voltage measurements performed in the nitrogen-filled glovebox. A 150 W xenon arc-lamp—Newport 96000—with an AM1.5G filter was used as the solar simulator with 100 mW/cm^2 power density. EQE measurements were performed using a tungsten halogen lamp source (250 W) with an Oriel Cornerstone 130 monochromator. TPV decay measurements were done using a Tektronix TDS 3054B oscilloscope equipped with a pulse laser light source (532 nm) under light bias from the solar simulator. Integrated photocurrent densities were obtained by calculating the product of the EQE and the AM1.5G spectra over the range of 370−1100 nm. A series of neutral density filters were used between the light source and the device to perform light intensity dependence measurements. A Keithley 4200-CVU system was used to record the capacitance−voltage data on a probe station with 100 mV ac signal amplitude in the range of −1 to 1 V and 50 kHz frequency.

ASSOCIATED CONTENT

Supporting Information

The Supporting Information is available free of charge at https://pubs.acs.org/doi/10.1021/acsami.9b18487.

Absorption spectrum of as-synthesized PbS QDs, semi-log dark *J-V* characteristics of the representative PbS QD PVs with Cu electrode with and without P3HT interlayer, series and shunt resistances of PbS QD devices with ultrathin Cu electrode with and without P3HT interlayer extracted from dark current measurements, evolution of other PV metrics for devices with Cu and Au electrodes under continuous illumination, PV characteristics of PbS QDS devices based on ultrathin Cu electrodes and P3HT interlayer with different thicknesses of PbS QDs measured under 100mW cm^{-2} AM1.5G illumination, PV characteristics of PbS QDs devices with ultrathin Cu electrodes with P3HT interlayer measured by illumination through Cu electrode and through ITO electrode, and PCE versus AVT diagram for Cu-based semi-transparent PbS QD PV as compared to the best performing PbS QDs devices (PDF)

AUTHOR INFORMATION

Corresponding Authors

*E-mail: hadit@mit.edu; haditavakoli.nano@gmail.com (H.T.D.).

*E-mail: mtavakol@mit.edu; mohmahtav2005@gmail.com (M.M.T.).

ORCID

Hadi Tavakoli Dastjerdi: 0000-0002-8925-5493

Zhiyong Fan: 0000-0002-5397-0129

Mohammad Mahdi Tavakoli: 0000-0002-8393-6028

Notes

The authors declare no competing financial interest.

ACKNOWLEDGMENTS

This work was supported by the Science and Technology Plan of Shenzhen (JCYJ20170818114107730), The IER foundation (no. 20170602), the National Natural Science Foundation of China (project no. 51672231), and the General Research Fund (project no. 16237816) from the Hong Kong Research Grant Council. H.T.D. thanks the support from the Natural Sciences and Engineering Research Council (NSERC) of Canada (award number: PDF-487850-2016). M.M.T. would like to acknowledge the Research Laboratory of Electronics (RLE) at Massachusetts Institute of Technology.

REFERENCES

(1) Chuang, C.-H. M.; Brown, P. R.; Bulović, V.; Bawendi, M. G. Improved Performance and Stability in Quantum Dot Solar Cells Through Band Alignment Engineering. *Nat. Mater.* **2014**, *13*, 796−801.

(2) Carey, G. H.; Levina, L.; Comin, R.; Voznyy, O.; Sargent, E. H. Record Charge Carrier Diffusion Length in Colloidal Quantum Dot Solids via Mutual Dot-To-Dot Surface Passivation. *Adv. Mater.* **2015**, *27*, 3325−3330.

DOI: 10.1021/acsami.9b18487
ACS Appl. Mater. Interfaces 2020, 12, 818−825

(3) Cao, Y.; Stavrinadis, A.; Lasanta, T.; So, D.; Konstantatos, G. The Role of Surface Passivation for Efficient and Photostable PbS Quantum Dot Solar Cells. *Nat. Energy* **2016**, *1*, 16035.
(4) Lan, X.; Voznyy, O.; de Arquer, F. P. G.; Liu, M.; Xu, J.; Proppe, A. H.; Walters, G.; Fan, F.; Tan, H.; Liu, M.; Yang, Z. 10.6% Certified Colloidal Quantum Dot Solar Cells via Solvent-Polarity-Engineered Halide Passivation. *Nano Lett.* **2016**, *16*, 4630−4634.
(5) Speirs, M. J.; Dirin, D. N.; Abdu-Aguye, M.; Balazs, D. M.; Kovalenko, M. V.; Loi, M. A. Temperature Dependent Behaviour of Lead Sulfide Quantum Dot Solar Cells and Films. *Energy Environ. Sci.* **2016**, *9*, 2916−2924.
(6) Crisp, R. W.; Kroupa, D. M.; Marshall, A. R.; Miller, E. M.; Zhang, J.; Beard, M. C.; Luther, J. M. Metal Halide Solid-State Surface Treatment For High Efficiency PbS and PbSe QD Solar Cells. *Sci. Rep.* **2015**, *5*, 9945.
(7) Tavakoli Dastjerdi, H.; Prochowic, D.; Yadav, P.; Tavakoli, M. M. Luminescence down-shifting enables UV-stable and efficient ZnO nanowire-based PbS quantum dot solar cells with J_{SC} exceeding 33 mA cm^{-2}. *Sustainable Energy Fuels* **2019**, *3*, 3128−3134.
(8) Zhang, Y.; Wu, G.; Mora-Seró, I.; Ding, C.; Liu, F.; Huang, Q.; Ogomi, Y.; Hayase, S.; Toyoda, T.; Wang, R.; Otsuki, J.; Shen, Q. Improvement of Photovoltaic Performance of Colloidal Quantum Dot Solar Cells Using Organic Small Molecule as Hole-Selective Layer. *J. Phys. Chem. Lett.* **2017**, *8*, 2163−2169.
(9) Tavakoli, M. M.; Mirfasih, M. H.; Hasanzadeh, S.; Aashuri, H.; Simchi, A. Surface Passivation of Lead Sulfide Nanocrystals with Low Electron Affinity Metals: Photoluminescence and Photovoltaic Performance. *Phys. Chem. Chem. Phys.* **2016**, *18*, 12086−12092.
(10) Tavakoli Dastjerdi, H.; Prochowicz, D.; Yadav, P.; Tavakoli, M. M. Synergistic Ligand Exchange and UV Curing of PbS Quantum Dots for Effective Surface Passivation. *Nanoscale* **2019**, *11*, 22832−22840.
(11) Tavakoli Dastjerdi, H.; Prochowicz, D.; Yadav, P.; Tavakoli, M. M. Tuning Areal Density and Surface Passivation of ZnO Nanowire Array Enable Efficient PbS QDs Solar Cells with Enhanced Current Density. *Adv. Mater. Interfaces* **2019**, 1901551.
(12) Liu, M.; Che, F.; Sun, B.; Voznyy, O.; Proppe, A.; Munir, R.; Wei, M.; Quintero-Bermudez, R.; Hu, L.; Hoogland, S.; Mandelis, A.; Amassian, A.; Kelley, S. O.; García de Arquer, F. P.; Sargent, E. H. Controlled Steric Hindrance Enables Efficient Ligand Exchange for Stable, Infrared-Bandgap Quantum Dot Inks. *ACS Energy Lett.* **2019**, *4*, 1225−1230.
(13) Aqoma, H.; Al Mubarok, M.; Hadmojo, W. T.; Lee, E.-H.; Kim, T.-W.; Ahn, T. K.; Oh, S.-H.; Jang, S.-Y. High-Efficiency Photovoltaic Devices using Trap-Controlled Quantum-Dot Ink prepared via Phase-Transfer Exchange. *Adv. Mater.* **2017**, *29*, 1605756.
(14) Kirmani, A. R.; Sheikh, A. D.; Niazi, M. R.; Haque, M. A.; Liu, M.; De Arquer, F. P. G.; Xu, J.; Sun, B.; Voznyy, O.; Gasparini, N.; Baran, D.; Wu, T.; Sargent, E. H.; Amassian, A. Overcoming the Ambient Manufacturability-Scalability-Performance Bottleneck in Colloidal Quantum Dot Photovoltaics. *Adv. Mater.* **2018**, *30*, 1801661.
(15) Zhang, X.; Öberg, V. A.; Du, J.; Liu, J.; Johansson, E. M. J. Extremely Lightweight and Ultra-Flexible Infrared Light-Converting Quantum Dot Solar Cells With High Power-Per-Weight Output Using a Solution-Processed Bending Durable Silver Nanowire-Based Electrode. *Energy Environ. Sci.* **2018**, *11*, 354−364.
(16) Kawawaki, T.; Wang, H.; Kubo, T.; Saito, K.; Nakazaki, J.; Segawa, H.; Tatsuma, T. Efficiency Enhancement of PbS Quantum Dot/ZnO Nanowire Bulk-Heterojunction Solar Cells by Plasmonic Silver Nanocubes. *ACS Nano* **2015**, *9*, 4165−4172.
(17) Jumabekov, A. N.; Cordes, N.; Siegler, T. D.; Docampo, P.; Ivanova, A.; Fominykh, K.; Medina, D. D.; Peter, L. M.; Bein, T. Passivation of PbS Quantum Dot Surface with L-Glutathione in Solid-State Quantum-Dot-Sensitized Solar Cells. *ACS Appl. Mater. Interfaces* **2016**, *8*, 4600−4607.
(18) Tavakoli Dastjerdi, H.; Tavakoli, R.; Yadav, P.; Prochowicz, D.; Saliba, M.; Tavakoli, M. M. Oxygen Plasma-Induced p-Type Doping Improves Performance and Stability of PbS Quantum Dot Solar Cells. *ACS Appl. Mater. Interfaces* **2019**, *11*, 26047−26052.
(19) Xu, J.; Voznyy, O.; Liu, M.; Kirmani, A. R.; Walters, G.; Munir, R.; Abdelsamie, M.; Proppe, A. H.; Sarkar, A.; García de Arquer, F. P.; Wei, M.; Sun, B.; Liu, M.; Ouellette, O.; Quintero-Bermudez, R.; Li, J.; Fan, J.; Quan, L.; Todorovic, P.; Tan, H.; Hoogland, S.; Kelley, S. O.; Stefik, M.; Amassian, A.; Sargent, E. H. 2D Matrix Engineering for Homogeneous Quantum Dot Coupling in Photovoltaic Solids. *Nat. Nanotechnol.* **2018**, *13*, 456−462.
(20) Jung, J. W.; Park, J.-S.; Han, I. K.; Lee, Y.; Park, C.; Kwon, W.; Park, M. Flexible and highly efficient perovskite solar cells with a large active area incorporating cobalt-doped poly(3-hexylthiophene) for enhanced open-circuit voltage. *J. Mater. Chem. A* **2017**, *5*, 12158−12167.
(21) Zhou, P.; Bu, T.; Shi, S.; Li, L.; Zhang, Y.; Ku, Z.; Peng, Y.; Zhong, J.; Cheng, Y.-B.; Huang, F. Efficient and stable mixed perovskite solar cells using P3HT as a hole transporting layer. *J. Mater. Chem. C* **2018**, *6*, 5733−5737.
(22) Zhang, X.; Zhang, J.; Liu, J.; Johansson, E. M. J. Solution Processed Flexible and Bending Durable Heterojunction Colloidal Quantum Dot Solar Cell. *Nanoscale* **2015**, *7*, 11520−11524.
(23) Kim, G.-W.; Kang, G.; Kim, J.; Lee, G.-Y.; Kim, H. I.; Pyeon, L.; Lee, J.; Park, T. Dopant-Free Polymeric Hole Transport Materials for Highly Efficient and Stable Perovskite Solar Cells. *Energy Environ. Sci.* **2016**, *9*, 2326−2333.
(24) Guo, Y.; Liu, C.; Inoue, K.; Harano, K.; Tanaka, H.; Nakamura, E. Enhancement in the efficiency of an organic-inorganic hybrid solar cell with a doped P3HT hole-transporting layer on a void-free perovskite active layer. *J. Mater. Chem. A* **2014**, *2*, 13827−13830.
(25) Shit, A.; Nandi, A. K. Interface Engineering of Hybrid Perovskite Solar Cells with Poly(3-Thiophene Acetic Acid) under Ambient Conditions. *Phys. Chem. Chem. Phys.* **2016**, *18*, 10182−10190.
(26) Nia, N. Y.; Matteocci, F.; Cina, L.; Di Carlo, A. High-efficiency Perovskite Solar Cell based on Poly(3-Hexylthiophene): Influence of Molecular Weight and Mesoscopic Scaffold Layer. *ChemSusChem* **2017**, *10*, 3854−3860.
(27) Joseph Kline, R.; McGehee, M. D.; Kadnikova, E. N.; Liu, J.; Fréchet, J. M. J.; Toney, M. F. Dependence of Regioregular Poly(3-Hexylthiophene) Film Morphology and Field-Effect Mobility on Molecular Weight. *Macromolecules* **2005**, *38*, 3312−3319.
(28) Zhang, X.; Hägglund, C.; Johansson, E. M. J. Highly Efficient, Transparent and Stable Semitransparent Colloidal Quantum Dot Solar Cells: A Combined Numerical Modeling and Experimental Approach. *Energy Environ. Sci.* **2017**, *10*, 216−224.
(29) Zhang, X.; Jia, D.; Hägglund, C.; Öberg, V. A.; Du, J.; Liu, J.; Johansson, E. M. J. Highly Photostable and Efficient Semitransparent Quantum Dot Solar Cells by Using Solution-Phase Ligand Exchange. *Nano Energy* **2018**, *53*, 373−382.
(30) Tavakoli, M. M.; Po, R.; Bianchi, G.; Cominetti, A.; Carbonera, C.; Camaioni, N.; Tinti, F.; Kong, J. A Relatively Wide-Bandgap and Air-Stable Donor Polymer for Fabrication of Efficient Semitransparent and Tandem Organic Photovoltaics. *Proc. Natl. Acad. Sci. U.S.A.* **2019**, *116*, 22037−22043.
(31) Tavakoli, M. M.; Nasilowski, M.; Zhao, J.; Bawendi, M. G.; Kong, J. Efficient Semitransparent $CsPbI_3$ Quantum Dots Photovoltaics Using a Graphene Electrode. *Small Methods* **2019**, *3*, 1900449.
(32) Roldán-Carmona, C.; Malinkiewicz, O.; Betancur, R.; Longo, G.; Momblona, C.; Jaramillo, F.; Camacho, L.; Bolink, H. J. High Efficiency Single-Junction Semitransparent Perovskite Solar Cells. *Energy Environ. Sci.* **2014**, *7*, 2968−2973.
(33) Choi, H.; Mai, C. K.; Kim, H. B.; Jeong, J.; Song, S.; Bazan, G. C.; Kim, J. Y.; Heeger, A. J. Conjugated Polyelectrolyte Hole Transport layer for Inverted-Type Perovskite Solar Cells. *Nat. Commun.* **2015**, *6*, 7348.

DOI: 10.1021/acsami.9b18487
ACS Appl. Mater. Interfaces 2020, 12, 818−825

(34) Yang, D.; Yang, R.; Zhang, J.; Yang, Z.; Liu, S.; Li, C. High efficiency flexible perovskite solar cells using superior low temperature TiO_2. *Energy Environ. Sci.* **2015**, *8*, 3208−3214.
(35) Tavakoli, M. M.; Simchi, A.; Fan, Z.; Aashuri, H. Chemical processing of three-dimensional graphene networks on transparent conducting electrodes for depleted-heterojunction quantum dot solar cells. *Chem. Commun.* **2016**, *52*, 323−326.
(36) Lu, K.; Wang, Y.; Liu, Z.; Han, L.; Shi, G.; Fang, H.; Chen, J.; Ye, X.; Chen, S.; Yang, F.; Shulga, A. G.; Wu, T.; Gu, M.; Zhou, S.; Fan, J.; Loi, M. A.; Ma, W. High-Efficiency PbS Quantum-DotSolar Cells with Greatly Simplified Fabrication Processing via "Solvent-Curing". *Adv. Mater.* **2018**, *30*, 1707572.
(37) Hu, L.; Geng, X.; Singh, S.; Shi, J.; Hu, Y.; Li, S.; Guan, X.; He, T.; Li, X.; Cheng, Z.; Patterson, R.; Huang, S.; Wu, T. Synergistic Effect of Electron Transport Layer and Colloidal Quantum Dot Solid Enable PbSe Quantum Dot Solar Cell Achieving Over 10% Efficiency. *Nano Energy* **2019**, *64*, 103922.
(38) Zhao, N.; Osedach, T. P.; Chang, L.-Y.; Geyer, S. M.; Wanger, D.; Binda, M. T.; Arango, A. C.; Bawendi, M. G.; Bulovic, V. Colloidal PbS Quantum Dot Solar Cells with High Fill Factor. *ACS Nano* **2010**, *4*, 3743−3752.
(39) Tavakoli, M. M.; Tayyebi, A.; Simchi, A.; Aashuri, H.; Outokesh, M.; Fan, Z. Physicochemical Properties of Hybrid Graphene−Lead Sulfide Quantum Dots Prepared by Supercritical Ethanol. *J. Nanopart. Res.* **2015**, *17*, 1−13.
(40) Tayyebi, A.; Tavakoli, M. M.; Outokesh, M.; Shafiekhani, A.; Simchi, A. Supercritical Synthesis and Characterization of Graphene-PbS Quantum Dots Composite with Enhanced Photovoltaic Properties. *Ind. Eng. Chem. Res.* **2015**, *54*, 7382.
(41) Tavakoli, M. M.; Aashuri, H.; Simchi, A.; Kalytchuk, S.; Fan, Z. Quasi Core/Shell Lead Sulfide/Graphene Quantum Dots for Bulk Heterojunction Solar Cells. *J. Phys. Chem. C* **2015**, *119*, 18886−18895.
(42) Tavakoli, M. M.; Simchi, A.; Aashuri, H. Supercritical Synthesis and in Situ Deposition of PbS Nanocrystals with Oleic Acid Passivation for Quantum Dot Solar Cells. *Mater. Chem. Phys.* **2015**, *156*, 163−169.

DOI: 10.1021/acsami.9b18487
ACS Appl. Mater. Interfaces 2020, 12, 818−825